Stellar Coronal Spectroscopy with the *Chandra HETGS*

David P. Huenemoerder [a]

[a]MIT Center for Space Research, 70 Vassar St., Cambridge, MA 02139

Grating spectra of cool stars from *Chandra* and *XMM-Newton* reveal a wealth of detail in their emission lines. Ability to resolve lines and detect the continuum allows detailed modeling of the temperature structure, abundances, and sometimes density. The abundances often show anomalies, such as strong neon and weak iron. Line strengths are often anomalous in flux ratios when compared to models or laboratory data. Temperature distributions are highly structured, but differ from star to star. I present qualitative results for a variety of objects: the pre-main sequence star TW Hya, which seems to be accretion driven, to neon-strong, iron-weak and highly variable RS CVn stars, II Peg, TY Pyx, and AR Lac, to the rapidly rotating giant, FK Com. I show detailed emission measures and abundance models for a few objects, as derived from line-based analysis of the coronal X-ray emission.

1. Cool Star X-ray Emission Modeling

The advent of high resolution X-ray spectra for objects other than the Sun allows us to test and extend our ideas on the nature of stellar coronae. We can now do a much better job in solving this:

$$f_l = \frac{A_{Z_l}}{4\pi d^2} \int \left[n_e n_H \frac{dV(T, n_e)}{d\log T} \right] \epsilon_l(T, n_e)\, d\log T$$

for the volume emission measure differential in temperature (square brackets; but for a given electron density, n_e) and elemental abundances (A_{Z_l}), given measured X-ray line fluxes, f_l (observed at distance d), and the emissivities, $\epsilon_l(T, n_e)$, as has been done with *EUV* spectra [2]. This does not tell us what the emission measure and abundances *mean* or how the emitting plasma is arranged; for interpretation we rely on constraints based on ensemble measurements, variability from eclipses, flares, and activity cycles, density diagnostics, and theoretical models which impose a geometry or temperature structure.

Figure 1 shows the results of simultaneously fitting abundances and differential emission measure (DEM) to many line fluxes measured in 200 ks of monitoring observations of IM Peg, a long period, single-lined, RS CVn binary. Uncertainties on the DEM and abundances are from Monte-Carlo fitting in which the observed fluxes were varied in accordance with their measurement uncertainties. The modeling does *not* account for uncertainties in the atomic data (APED; [11]) or assumed ionization balance [7]. Since the solution is very under-determined, regularization is done by smoothing the DEM slightly.

Figure 2 shows the DEM solution for AR Lac, which had distinct flares during the observations. The DEM structure is very similar to that obtained for IM Peg. The bottom pane of Figure 2 shows the observed line-modulation ($[max-min]/[max+min]$) which shows that variability occurred primarily at high temperatures, consistent with the observation of flares.

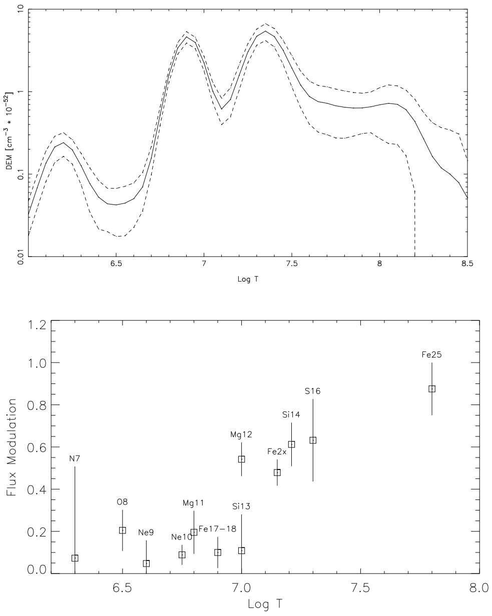

Figure 2. AR Lac, emission measure (top), and line modulation vs. temperature of peak emissivity (bottom), derived from six *HETGS* observations.

It is important to be able to easily synthesize and inspect spectra in detail, and to easily "kick"

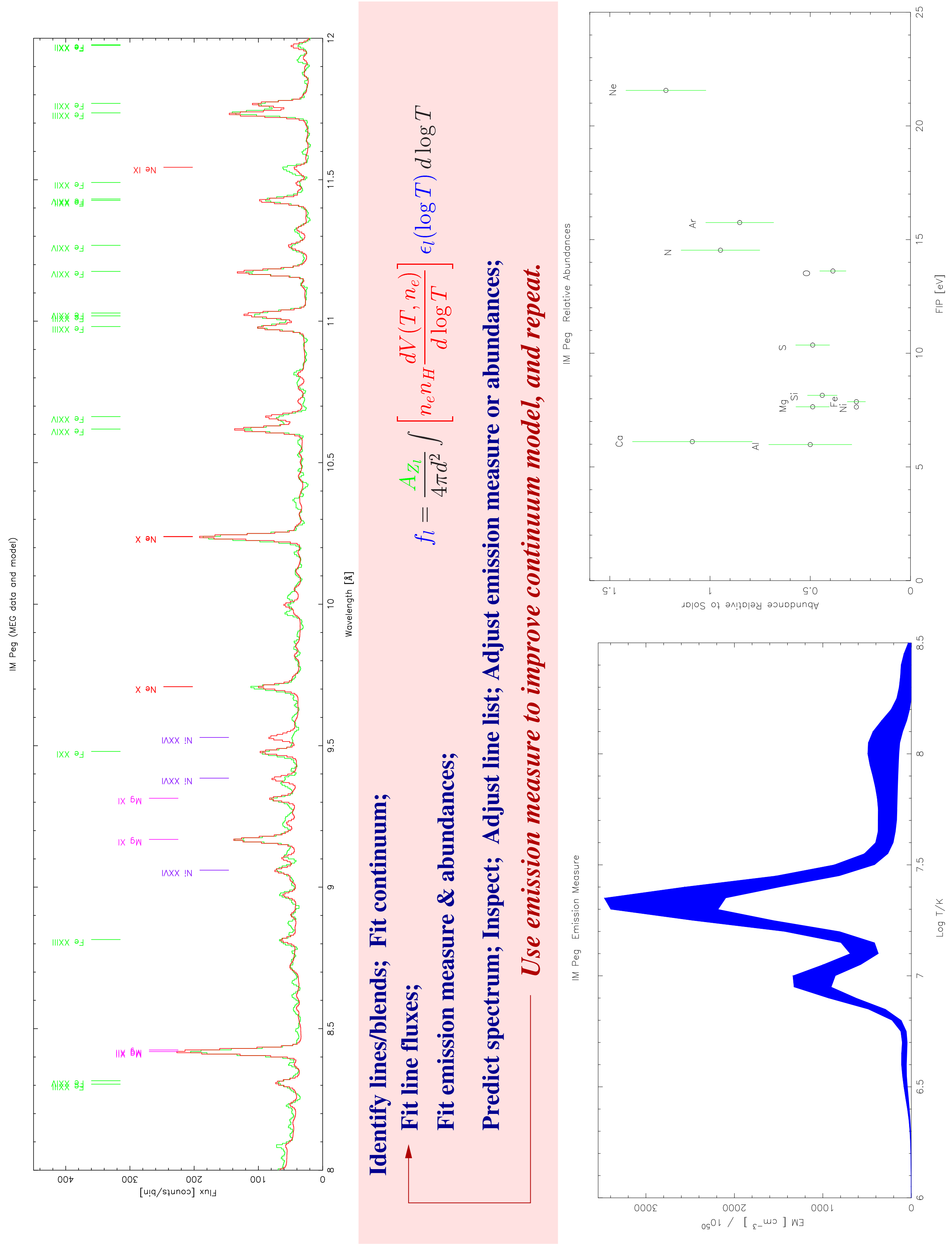

Figure 1. IM Pegasi, synthetic *MEG* counts spectrum (top: red, smooth) and data (green), emission measure (bottom left; solid region is one-sigma boundary), and abundances vs. first ionization potential (FIP; bottom right).

the solution. Figure 3 shows the result after *ad hoc* adjustment of the Ca abundance, since the blind fit gave more weight to the *MEG* counts — for which the line looks weak or non-existent — or to stronger lines. *Resolution* is also important, as seen by comparing Ca XIX (3.2 Å) in the upper (*HEG*, higher resolution, but less sensitivity) and lower graphs (*MEG*). Since the primary species labeled (S, Ar, Ca) have strongly overlapping emissivities (see inset), the discrepant Ca emission could not be adjusted via changes in the DEM, but had to be are result of a poor fit to the abundance.

After a model has been obtained, iterations are performed which include newly identified features, or excluding clearly mis-identified or too-blended lines, and by also using the physical continuum to improve line measurement in crowded or noisier regions. The importance of line-based fitting, of continuum prediction and measurement, and of ability to inspect the database to resolve blends and to find and measure weaker features, cannot be over-emphasized. There are no global fit black-boxes for high resolution emission line spectral modeling.

2. Cool Star X-ray Emission in Context

Since we don't yet have an a priori theory to reliably predict coronal X-ray emission even for the Sun or Solar-type stars [8], we are obligated to observe many objects in different evolutionary states or of different fundamental parameters, or just at different times. I have collected a dozen stellar spectra, most now in the public archives, spanning a wide range in period as well as other parameters. They range from the Classical T Tauri star, TW Hya [6], the very short period dwarf binaries, 44 Boo [3] and AB Dor [10], classical RS CVn stars like HR 1099 and UX Ari, to long period RS CVn binaries like λ And, [1,4,10], and the eponymous FK Com [5]. A small portion of their spectra are displayed in Figure 4. The region includes the He-like Ne IX triplet at 13.5 Å, and the principal Fe XVII line at 15 Å. These have similar emissivity distributions with temperature, so their ratio is a qualitative Ne:Fe abundance ratio diagnostic. I have arranged them from high Ne:Fe to low from top to bottom. It is clear that there is a rather continuous range. It is also clear that TW Hya is unique in having a strong forbidden line, which has been interpreted as indicative of high density[6].

I show the variability of these same systems in Figure 5, which shows the phased light curves of the diffracted photons (zero orders are usually saturated). *Every single one is variable.* The top curve is for all diffracted photons, and the lower trace is for low-temperature lines. Almost all the modulation is due to the high temperature component, indicating that the variability is due to temperature changes (flaring), as opposed to rotational modulation (visible emitting volume). The only obvious exception is TY Pyx, which clearly shows a primary eclipse. AR Lac, a totally eclipsing binary, has too much intrinsic variability to see the eclipse, a conclusion also reached by [9]. The short-period system, 44 Boo, shows marginal evidence for eclipse modulation at zero phase [3]. IM Peg was monitored with *HETGS* for two rotations with the intent of detecting geometric modulation. However, the amplitude variations did not repeat (different rotations are plotted in different colors in both upper and lower graphs), indicating that its slow variability is probably from long duration flares.

3. Conclusions

We can now model in some detail *HETGS* spectra to provide temperature distributions and abundances which provide excellent matches to observed spectra. It seems clear that most variability is due to flares and not rotational modulation; the hot peak in DEM solutions ($\log T \sim 7.4$) as well as the hot tail ($\log T > 7.4$) are probably primarily due to flaring. Discerning rotational and eclipse modulation in the midst of the frequent flaring will require intensive monitoring observations. Interpretation of the abundance trends will require much work, comparing to photospheric abundances, activity levels, or plasma modeling systematic errors (including ionization balance and equilibrium assumptions).

Without a physical theory, interpretation of the emission measure and abundances is difficult. We must rely on ensemble measurements we are now obtaining which provide contexts for the emission for a wide variety of sources. We must support a variety of analysis methods since each is sensitive to different parameters, has slightly different model assumptions, or different biases. In this conference alone, we can see several good examples of different approaches (see the contri-

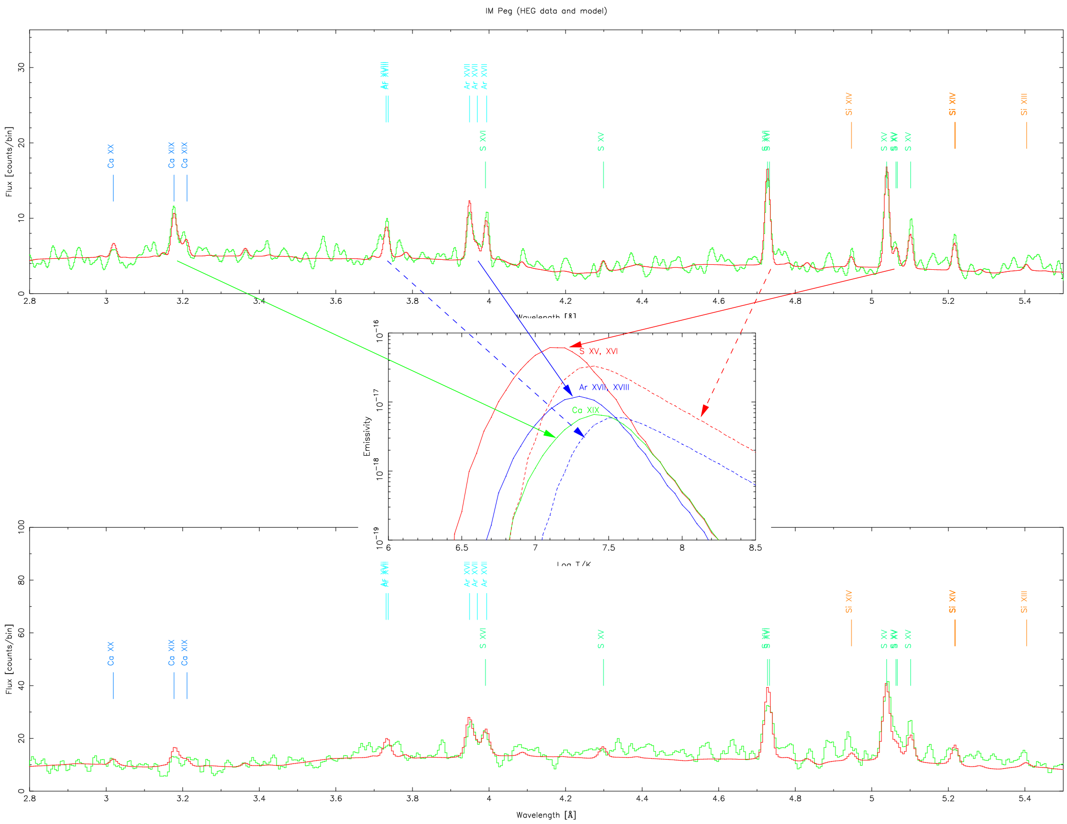

Figure 3. IM Pegasi, synthetic *MEG* counts (smooth, red) and observed counts (jagged, green), for *HEG* (top) and *MEG* (bottom) gratings. Line emissivities for S, Ar, and Ca are inset.

butions of Audard; Güdel; Schmitt; Ness; Wojdowski.[1] We expect that continued work with grating spectra will lead to better understanding of the energy deposition into stellar coronae and the dependence upon fundamental stellar parameters and evolutionary state.

REFERENCES

1. Ayres, T. R., Brown, A., Osten, R. A., Huenemoerder, D. P., Drake, J. J., Brickhouse, N. S., & Linsky, J. L., 2001, ApJ, 549, 554
2. Bowyer, S., Drake, J. J., & Vennes, S. ., 2000, ARA&A, 38, 231
3. Brickhouse, N. S., Dupree, A. K., & Young, P. R., 2001, ApJ, 562, L75
4. Drake, J. J., Brickhouse, N. S., Kashyap, V., Laming, J. M., Huenemoerder, D. P., Smith, R., & Wargelin, B. J., 2001, ApJ, 548, L81
5. Gondoin, P., Erd, C., & Lumb, D., 2002, A&A, 383, 919
6. Kastner, J. H., Huenemoerder, D. P., Schulz, N. S., Canizares, C. R., & Weintraub, D. A., 2002, ApJ, 567, 434
7. Mazzotta, P., Mazzitelli, G., Colafrancesco, S., & Vittorio, N., 1998, A&AS, 133, 403
8. Parker, E. N., 1998, Advances in Space Research, 21, 267
9. Pease, D., et al., 2002, in ASP Conf. Ser. 277: Stellar Coronae in the Chandra and XMM-Newton Era, Vol. 277, 547
10. Sanz-Forcada, J., Brickhouse, N. S., & Dupree, A. K., 2002, ApJ, 570, 799
11. Smith, R. K., Brickhouse, N. S., Liedahl, D. A., & Raymond, J. C., 2001, ApJ, 556, L91

ACKNOWLEDGEMENTS

This work was supported by NASA through the CXC contract to MIT, SAO SV1-61010, and by Chandra Award Number GO2-3005A issued by the CXC, operated by SAO for and on behalf of NASA contract NAS8-39073.

[1] `http://www.mssl.ucl.ac.uk/~gbr/rgs_workshop/workshop_ADS_index.html`

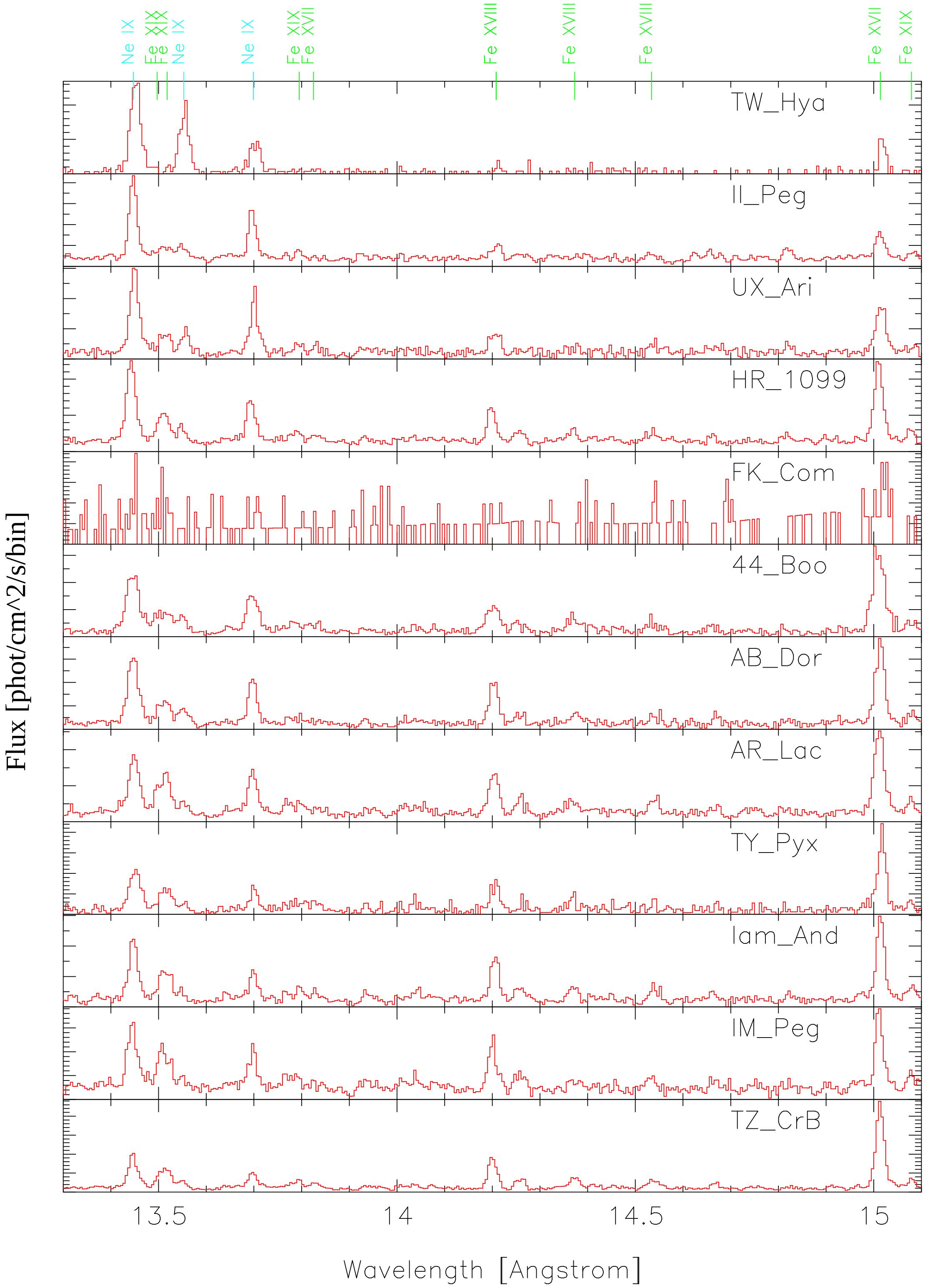

Figure 4. Gallery of spectra, for a very diverse collection of cool stars. The Ne IX triplet lines (13.44, 13.55, 13.70 Å) are at the left, and Fe XVII, which has a similar emissivity distribution with temperature, is at the right (15.02 Å). Spectra have been ordered by relative strength of Ne IX to Fe XVII, a mainly abundance-dependent ratio.

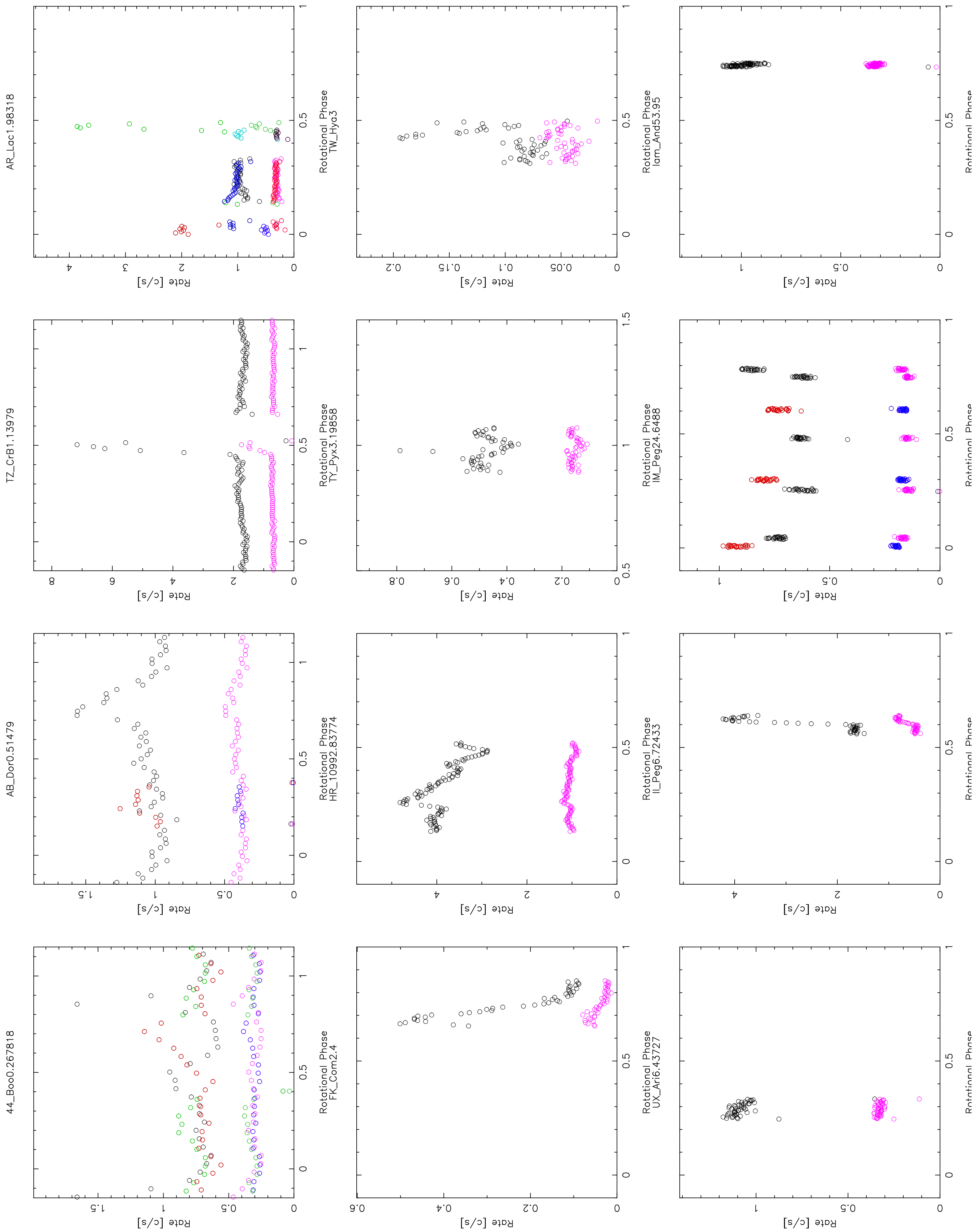

Figure 5. A gallery of phased light curves for the same cool stars shown in Figure 4. They are arranged from short (0.25 day) to long (53 day) periods, left-to-right and top-to-bottom (when viewed in landscape orientation). Uncertainties are on the order of (or less than) the symbol size. Upper curves are for all diffracted photons, lower are for low-temperature lines. Different rotations are plotted in different colors. (Note: ignore erroneous points near a rate of zero, which are artifacts of poor accounting of good-time boundaries.)